Microscopic model for the strain-driven direct to indirect band-gap transition in monolayer MoS_2 and ZnO

Ruma Das, Bipul Rakshit, Saikat Debnath, and Priya Mahadevan
Department of Condensed Matter Physics and Material Science, SN Bose National Centre for Basic Sciences, Block JD, Sector III, Salt Lake, Kolkata 700 098, India
(Received 22 May 2013; revised manuscript received 13 February 2014; published 6 March 2014)

At the monolayer limit both MoS_2 and the graphitic phase of ZnO have a direct band gap. Biaxial tensile strain has been found to induce a transition into an indirect band-gap semiconductor with the strain percentage required for the transition equal to 0.83% for MoS_2 and 8% for ZnO, respectively. A low strain percentage is desirable for possible device applications. We identify a simple design principle which could be used to identify materials requiring a small strain to induce such a transition. A scaling of the hopping interaction strengths according to Harrison's law within a tight-binding model for MoS_2 is able to capture the effect.

DOI: 10.1103/PhysRevB.89.115201 PACS number(s): 63.22.Np, 73.22.−f, 71.20.Nr

I. INTRODUCTION

The isolation of the first two-dimensional crystal, graphene [1,2], generated a huge interest in the study of these materials. A major focus of the research on graphene has been on possible applications in the electronics industry [3–5] with the approach to tune the properties that have been adopted, to be by doping [6]. However, the absence of a band gap has limited its applications and shifted the focus onto several layered transition-metal disulphides and diselenides such as MoS_2, WSe_2, etc., [7–10]. MoS_2 has been found to have a bulk band gap of 1.29 eV [11], which is an indirect one. A single monolayer, on the other hand, is found to have a direct band gap which is 1.9 eV [12,13]. Similar thickness-dependent changes from a direct band-gap semiconductor to an indirect band-gap semiconductor have been seen in other materials such as (Mo/W)X_2 (X = S, Se, and Te) [14] and ZnO [15]. Recently strain has been shown to be an important parameter in tuning the band gap. Varying the strain from 0% to 9%, the magnitude of the band gap has been found to change by almost 1 eV or more in MoS_2 [16], depending on the choice of the exchange-correlation functionals used. In addition a strain-dependent direct to indirect band-gap transition was found even at a modest value of the strain [17,18]. The strain-dependent direct to indirect band-gap transition has been seen in other transition-metal dichalcogenides also [19].

In this work we consider the case of two materials, MoS_2 and ZnO, which represent contrasting limits of their behavior under biaxial tensile strain at the monolayer limit and study the variation of the band gap. In both cases one has a direct band gap at zero strain. Under biaxial tensile strain, a transition is found to take place at just 0.83% in MoS_2 to an indirect band-gap material. However, a strain of 8% is required in the case of ZnO. Modest values of strain for bringing about the crossover are preferable for use in various devices, and so it would be useful to have a microscopic understanding of the differences in the critical strain required in the two systems.

In order to understand this, we mapped the *ab initio* band structure onto a tight-binding model. The highest occupied band at the **Γ** point in MoS_2 is found to emerge from Mo d–S p interactions, while that at the **K** point emerges from Mo d–Mo d interactions. The fact that we have two different sets of interactions contributing to the highest occupied band at the two symmetry points suggests the role that strain can play in changing the valence band maxima position. The distance (r) dependence of the hopping interactions are expected to vary as $1/r^{l+l'+1}$ from an empirical scaling law put forth by Harrison [20]. Here l and l' are the angular momenta of the orbitals which are involved. Accompanying the strain-induced modifications of the interaction strengths, one also has a charge transfer between the atoms involved. Accounting for these two aspects we find that our tight-binding model can capture the strain-driven direct to indirect band-gap transition found in MoS_2. Moving on to the case of ZnO, we find that the highest occupied band at the **Γ** and **K** points are both contributed by Zn d–O p interactions. Hence, as the same set of interactions contribute to both symmetry points, tunability to the extent possible in MoS_2 cannot be achieved here, as biaxial tensile strain modifies the energies of the valence-band maximum (VBM) at both symmetry points to almost the same extent. Hence the present paper provides a facile route to identify systems which can be suitable for band-gap engineering via strain. The ideas are then tested for three other systems, $MoSe_2$, WSe_2, and BN, with success in each case.

II. METHODOLOGY

The electronic structure of MoS_2 and ZnO have been calculated within a plane wave pseudopotential implementation of density functional theory using the VASP [21] code. The experimental crystal structure [22] has been taken in the case of MoS_2 and a vacuum of 20 Å was used between successive MoS_2 monolayers to minimize interactions between images in the periodic supercell method that we use. While the lattice parameters were kept fixed at the experimental values [22], the internal positions were optimized in each case. Projected augmented wave [23,24] potentials were used to solve the electronic structure self-consistently using a k-points mesh of $12 \times 12 \times 1$ with a cutoff energy for the plane wave basis states equal to 450 eV to achieve a total energy convergence of 5 meV or less. Perdew-Burke-Ernzerhof [25] potentials were used for the exchange-correlation functionals and the calculations were performed as a function of biaxial tensile strain. The transition from direct to indirect band-gap semiconductor were contrasted with the results for the ZnO monolayer. We have

 ©2014 American Physical Society

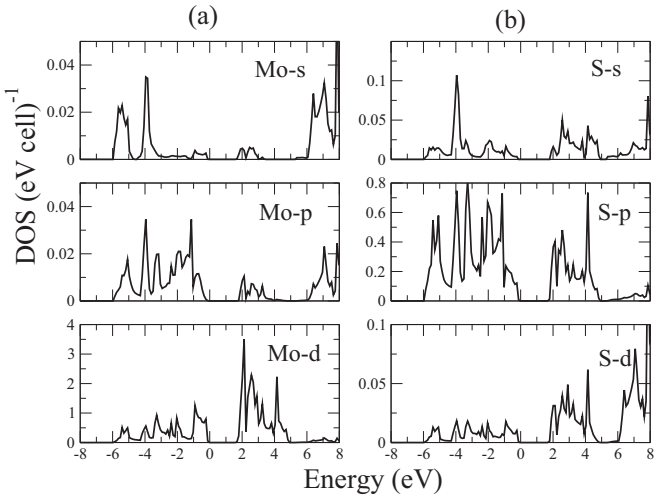

FIG. 1. The atom and angular momentum projected partial density of states for (a) Mo and (b) S atoms from *ab initio* calculations using generalized gradient approximation (GGA) potentials. Zero of energy corresponds to the Fermi energy.

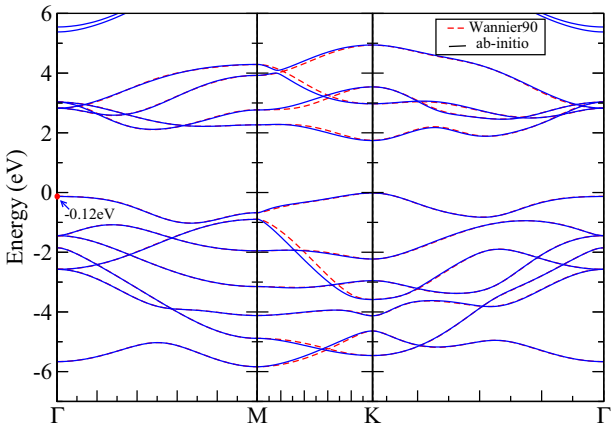

FIG. 2. (Color online) *Ab initio* band dispersions (solid line) for monolayer MoS_2 at its experimental lattice constant (0% biaxial tensile strain), using GGA potentials. The fitted tight-binding bands (dashed line), using a basis consisting of Mo d and S p have been superposed. Here the radial part of the tight-binding basis functions correspond to maximally localized Wannier functions. The zero of energy is the valence band maximum.

used the experimental lattice constant, $a = 3.099$ Å for a monolayer of ZnO [26]. The details of the calculations are similar to what was done for MoS_2 except that one used LDA + U potentials with a U of 8 eV on the Zn d states. A U of 8 eV has been found to be necessary [27] for correcting the self-interaction error. Additionally we used plane waves with kinetic energy less than 450 eV in the basis. In the absence of this correction, one has a significant admixture of Zn d states in the valence band. The phonon dispersions for ZnO were calculated using a $4 \times 4 \times 1$ supercell. The small displacement method was used for the calculation of phonons [28]. The longitudinal optical–transverse optical splitting is not included in the calculated phonon dispersions. The *ab initio* band structures calculated at 0% biaxial tensile strain as well as at 2% biaxial tensile strain for MoS_2 were mapped onto a tight-binding model for carrying out further analysis. In order to determine the appropriate basis functions to be included on Mo and S, the Mo s,p,d as well as S s,p,d contributions to the partial density of states are shown in Fig. 1. We find that the dominant contributions are from Mo d as well as S p states with nonzero contributions from other states. Initially we considered a model with Mo d and S p states in the basis. The radial parts of the basis functions were considered to be maximally localized Wannier functions [29]. All on-site energies and hopping interaction strengths in this case were determined from the interface of VASP to WANNIER90 [30]. While an excellent mapping of the *ab initio* band structure was obtained within the model Hamiltonian, one found that the extracted values of the hopping interaction strengths depended on the pair of orbitals considered, making a mapping onto a consistent set of Slater-Koster parameters difficult. In another model that we considered, we included the Mo s,p,d as well as the S s,p,d states in the basis. The tight-binding parameters were determined by a least-square error minimization. A Harrison's type scaling [20] of the hopping integrals of the form $1/r^{l+l'+1}$ has been assumed for the Mo d–Mo d as well as the Mo d–S p interactions for deviations up to 0.1 Å, about the distance at which the hopping interaction strength is defined. The ideas built from our analysis for ZnO and MoS_2 were used to examine the band-gap dependence under strain of $MoSe_2$ and WSe_2 as well as boron nitride (BN). The lattice constants used were 3.254, 3.325, and 2.511 Å for $MoSe_2$ [31], WSe_2 [31], and BN [32], respectively, and we used plane wave cutoff energies of 450 eV for the basis set in the calculations.

III. RESULTS AND DISCUSSIONS

The band dispersions calculated along various symmetry directions for monolayer MoS_2 are given in Fig. 2. The VBM is found to be at the **K** point, while the highest occupied band at **Γ** is found to be 0.12 eV lower. The conduction band bottom is found to be at the **K** point. Hence, consistent with experiment, one finds a direct band gap of 1.76 eV in MoS_2 in our calculations. This value is slightly underestimated from the experimental value of 1.9 eV [12,13]. Although an underestimation of the band gap is a well-known drawback of the density functional theory based calculations, the small underestimation here seems fortuitous. We then go on to examine the nature of the interactions that contribute to the VBM at both symmetry points **Γ** and **K**. This is done by examining the charge density at these two symmetry points. As evident from Fig. 3(a), the highest occupied band at the **Γ** point is found to emerge from the interactions between the d_{z^2} orbitals on Mo and the p_z orbitals on S. The highest occupied band at the **K** point is, on the other hand, derived from direct d-d interactions between the Mo atoms in the plane, which is shown in Fig. 3(b).

We then went on to examine the effect of biaxial tensile strain on the electronic structure of MoS_2. At a biaxial tensile strain of 2% (Fig. 4), we find that the highest occupied band shifts to **Γ**, while the lowest unoccupied band remains at the **K** point. The highest occupied band at the **K** point is now 0.14 eV lower than that at the **Γ** point. Hence biaxial tensile strain

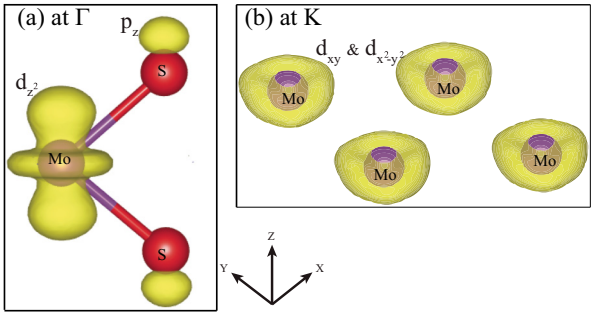

FIG. 3. (Color online) The charge density plot for monolayer MoS_2 for the highest occupied band at (a) **Γ** and (b) **K** symmetry points obtained from *ab initio* calculations using GGA potentials at 0% strain.

has been found to drive a transition from a direct band-gap semiconductor into an indirect band-gap semiconductor as has been seen earlier [17,18]. We then go on to examine what are the changes that take place in the bond lengths under strain. A 2% biaxial tensile strain is found to change the in-plane first neighbor Mo-Mo bond lengths from 3.16 to 3.22 Å, while the Mo-S bond lengths change only marginally from 2.41 to 2.42 Å. This has the effect of decreasing the Mo-Mo interactions while not having any effect on the Mo-S interaction. As a result, the highest occupied band at the **K** point, which is derived from Mo-Mo interactions, moves deeper into the valence band and is no longer the location of the VBM for the system. As a result we have the observed transition from a direct to an indirect band-gap semiconductor.

In order to understand the role of various microscopic interactions in bringing about the crossover, we have used the VASP to WANNIER90 interface to map the *ab initio* band structure onto a tight-binding model with Mo d and S p states as the basis functions. The fitted tight-binding bands are superposed on the *ab initio* bands in both Figs. 2 and 4 for the unstrained case as well as the 2% strained case. In both cases, one finds that one has a good description of the *ab initio* band structure within the tight-binding model. The wave function corresponding to the highest occupied band at the **K** point is found to have 38% weight on Mo $d_{x^2-y^2}$ and 40% on d_{xy} within our tight-binding model. At the **Γ** point the weight is found to be 64% on Mo $d_{3z^2-r^2}$ and the remaining is on S p_z orbitals. We go on to analyze which are the microscopic interactions that are responsible for the system becoming an indirect band-gap semiconductor. While at 0% biaxial tensile strain, the VBM at the **K** point is 0.12 eV higher than that at the **Γ** point, one finds that under 2% biaxial tensile strain the VBM at the **Γ** point is 0.14 eV higher than that at the **K** point. Hence we have a net movement of 0.26 eV of the energy at the **Γ** point with respect to the energy at the **K** point. Using the tight-binding Hamiltonian for the unstrained case we find that replacing the on-site energies with those obtained in the 2% strained case gives us a relative shift of 0.06 eV, just 25% of the observed shift. Using a Harrison-type scaling of the hopping interaction strengths as well as the modified on-site energies does not give us the required shift that one finds in the *ab initio* calculations. Closer analysis reveals that the hopping interaction strengths have a complicated distance dependence. However, it is clear from this analysis that they contribute to 75% of the energy lowering bringing about the change from a direct band-gap semiconductor to an indirect band-gap semiconductor.

We then go on to examine if the deviations from a Harrison-type scaling law [20] found in the tight-binding model using maximally localized Wannier functions as the basis, is a consequence of using a limited set of basis states which includes Mo d and S p states. In order to examine that we considered a tight-binding model with Mo s,p,d as well as S s,p,d states in the basis. The *ab initio* band structure as well as the tight-binding band structure are given in Fig. 5 for 0% strain. A similar analysis is done for 2% strain also where we kept the Mo d–S p as well as Mo d–Mo d interactions fixed at their zero strain values and allowed them to scale with distance according to a

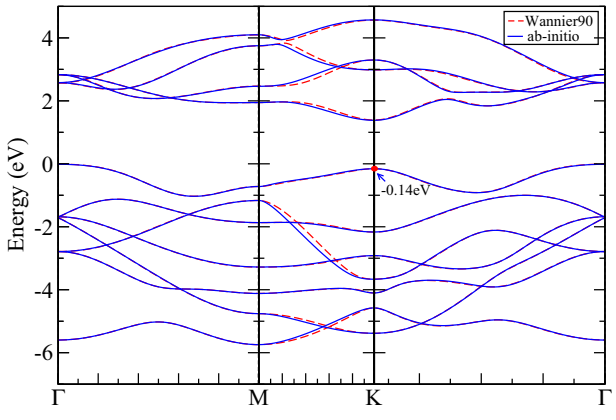

FIG. 4. (Color online) *Ab initio* band dispersions (solid line) for monolayer MoS_2 at its experimental lattice constant (2% biaxial tensile strain), using GGA potentials. The fitted tight-binding bands (dashed line), using a basis consisting of Mo d and S p have been superposed. Here the radial part of the tight-binding basis functions correspond to maximally localized Wannier functions. The zero of energy is the valence band maximum.

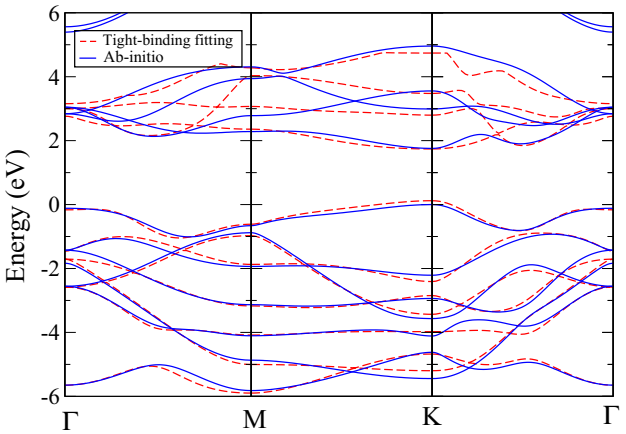

FIG. 5. (Color online) Comparison of *ab initio* band dispersions (solid line) for monolayer MoS_2 at its experimental lattice constant (0% biaxial tensile strain), using GGA potentials and the fitted tight-binding bands (dashed line), using a basis consisting of Mo s,p,d and S s,p,d states. The zero of energy is the valence band maximum.

TABLE I. Parameters obtained from least-squared-error fitting of the *ab initio* band structure onto a tight-binding model using *s*,*p*,*d* orbitals of Mo and S for monolayer MoS_2 at 0% biaxial tensile strain. The energies are in eV.

	E_s	E_p	E_d
S	3.9894	6.9128	2.0629
Mo	6.8495	−3.3237	9.0089
	E(Mo,Mo)	E(Mo,S)	E(S,S)
$ss\sigma$	0.8268	−2.1317	0.0993
$sp\sigma$	1.4510	−2.2315	−0.1710
$sd\sigma$	−0.1335	−0.9754	−0.0016
$pp\sigma$	−0.0042	1.7208	0.3032
$pp\pi$	0.9503	−1.0012	−0.2020
$pd\sigma$	−0.0716	3.8098	−0.8904
$pd\pi$	0.0182	−3.2608	−0.0003
$dd\sigma$	0.1702	−3.2825	0.0647
$dd\pi$	0.0032	2.3575	0.5034
$dd\delta$	0.1508	−0.2603	−0.9719
$ps\sigma$	−1.4510	0.1756	0.1710
$ds\sigma$	0.1335	0.4977	0.0016
$dp\sigma$	0.0716	−2.8432	0.8904
$dp\pi$	−0.0182	1.0539	0.0003

Harrison-type scaling law. Other parameters were allowed to vary within reasonable limits. The fitted parameters are given in Table I for the 0% case and in Table II for the 2% case considered. Here E_s, E_p, and E_d are the on-site energies for the s, p, and d levels on the atoms considered. The hopping interaction strengths have been parametrized in terms of the Slater-Koster parameters for Mo-Mo [E(Mo,Mo)], Mo-S [E(Mo,S)], and S-S [E(S,S)]. A comparison of the band structure from the tight-binding calculation with the *ab initio* band structure for 2% is shown in Fig. 6, and a good fit has been obtained. This shows

TABLE II. Parameters obtained from least-squared-error fitting of the *ab initio* band structure onto a tight-binding model using *s*,*p*,*d* orbitals of Mo and S for monolayer MoS_2 at 2% biaxial tensile strain. The energies are in eV.

	E_s	E_p	E_d
S	3.5494	6.6528	2.1829
Mo	6.0195	−3.8237	8.7189
	E(Mo,Mo)	E(Mo,S)	E(S,S)
$ss\sigma$	0.9868	−2.3417	0.0093
$sp\sigma$	1.4110	−2.0115	−0.2010
$sd\sigma$	0.0135	−0.7954	−0.0016
$pp\sigma$	0.0042	1.5108	0.4132
$pp\pi$	1.0303	−0.9412	−0.2020
$pd\sigma$	−0.1516	3.9098	−0.8004
$pd\pi$	0.0082	−3.3907	−0.0203
$dd\sigma$	0.1702	−3.4125	0.4147
$dd\pi$	0.0032	2.5175	0.3334
$dd\delta$	0.1508	−0.1603	−0.9919
$ps\sigma$	−1.4110	0.3956	0.2010
$ds\sigma$	0.0135	0.2177	0.0016
$dp\sigma$	0.1516	−2.8432	0.8004
$dp\pi$	−0.0082	1.0539	0.0203

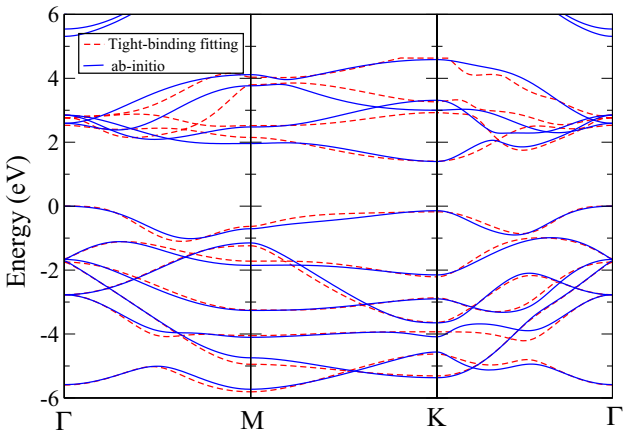

FIG. 6. (Color online) Comparison of *ab initio* band dispersions (solid line) for monolayer MoS_2 at its experimental lattice constant (2% biaxial tensile strain), using GGA potentials and the fitted tight-binding bands (dashed line), using a basis consisting of Mo *s*,*p*,*d* and S *s*,*p*,*d* states. The zero of energy is the valence band maximum.

that the strain-driven direct to indirect band-gap transition can be described in terms of scaling of the interaction strengths assuming a dependence that was first proposed by Harrison.

To compare with MoS_2 we considered another layered material, ZnO. This has recently been shown to exist in a metastable phase [26] and few monolayers on various substrates have been found to favor a graphitic phase [33]. The band dispersions are plotted in Fig. 7, along various symmetry directions for monolayers of ZnO. Here we also find that it is a direct band-gap material with its VBM at the **Γ** point. The lowest unoccupied band is also at the **Γ** point and we find a band gap of 2.71 eV. This is underestimated from the value of 3.25 eV obtained from hybrid functional calculations, which we compare with in the absence of experimental information for the band gap. However we do not perform hybrid functional calculations as a function of strain as it has been seen earlier [15] that qualitative aspects are captured by LDA + U calculations which are computationally less demanding. The large separation of 0.60 eV between the highest occupied band

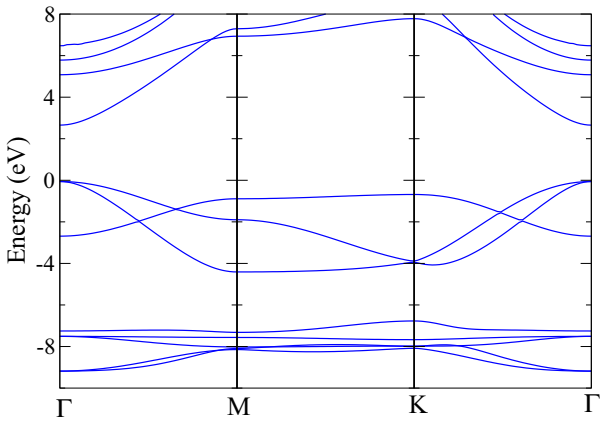

FIG. 7. (Color online) *Ab initio* band dispersions for monolayer ZnO within LDA + U, U = 8 eV at its experimental lattice constant. The zero of energy is the valence band maximum.

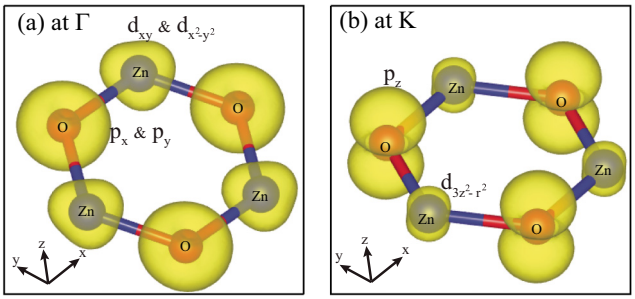

FIG. 8. (Color online) The charge density plot for monolayer ZnO for the highest occupied band at (a) **Γ** and (b) **K** high-symmetry points. obtained from *ab initio* calculations using LDA + U, U = 8 eV potentials at 0% strain.

at the **Γ** point and that at the **K** point immediately suggests that strain cannot be used as a parameter to tune the band gap so effectively here. Examining the character of the highest occupied band at the **Γ** point and that at the **K** point we find that the band at the **Γ** point is contributed by Zn d–O p interactions involving the in-plane Zn d orbitals and p_x/p_y orbitals on oxygen. The **K** point, on the other hand, is contributed by Zn $d_{3z^2-r^2}$ orbitals interacting with p_z orbitals on oxygen as is evident from the charge density plotted in Fig. 8. Both symmetry points are contributed by interactions between the Zn d and O p orbitals. So as there are similar shifts expected with biaxial tensile strain at both symmetry points, one finds that the strain tunability is small. In Fig. 9 we have plotted the energy gap as a function of biaxial tensile strain for the case where the highest occupied band at the **K** point is considered, in addition to the conduction band bottom is at the **Γ** point. This is denoted as the energy gap **KΓ**. We have also plotted the direct band gap at **ΓΓ** between the highest occupied band at **Γ** and the lowest unoccupied band also at the **Γ** point. Up to a biaxial tensile strain of 8% one finds that the direct band gap is smaller than the indirect one. The **KΓ** energy gap becomes the smaller band gap for values of biaxial tensile strain greater than 8%. We have calculated the phonon spectrum at a strain

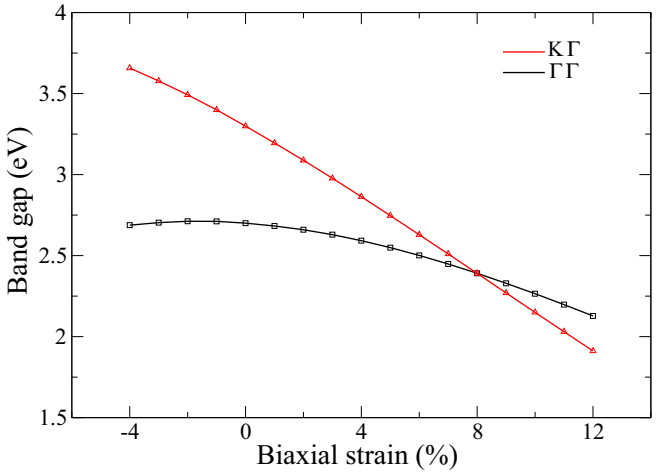

FIG. 9. (Color online) The variation of the direct and the indirect band gap for monolayer ZnO at various biaxial tensile strain obtained within *ab initio* calculations using LDA + U, U = 8 eV potentials.

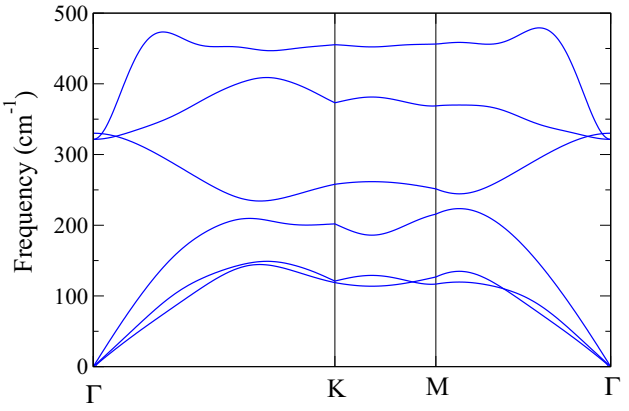

FIG. 10. (Color online) The calculated phonon dispersion for ZnO at 10% biaxial tensile strain along various symmetry directions.

percentage of 10%, which is shown in Fig. 10 and we find the phonon modes to be positive. This indicates that the structure is stable even when subjected to such a large strain.

The study for MoS_2 and ZnO has provided a simple route to systems in which band-gap engineering from a direct to an indirect band-gap semiconductor is possible. We consider two other systems, $MoSe_2$ and WSe_2, which have a structure similar to MoS_2 and find that at the experimental lattice parameters, the highest occupied band (VBM) at the **Γ** and **K** points differ by 0.365 and 0.42 eV (Table III). Hence a modest strain of ∼3% (Table III) is able to bring about the transition from a direct band-gap semiconductor to an indirect band-gap semiconductor. While at first sight, the differences in the two systems studied could be directly linked to the structure involved, we consider the third case to be BN which has a structure similar to ZnO, which we had studied earlier. In contrast to ZnO, here we find that the lowest unoccupied band (CBM) at the **Γ** point is 0.094 eV lower than the lowest occupied at the **K** point using the experimental lattice parameters. However, from an analysis of the character of these points we find that the **Γ** point is contributed by interactions between N-s states, while one finds that the **K** point emerges from B-p interactions. Hence as the hopping interaction strengths scale as $1/r^{l+l'+1}$, the CBM at **Γ** and **K** move at different rates under strain. Hence a transition is found at a modest value of strain of 2%.

An alternate approach to understanding the strain-driven direct to indirect band-gap crossover is by examining the deformation potentials. These are shown for different materials in Table IV. Examining the values for MoS_2 at the **Γ** and **K**

TABLE III. Strain percentage at which the band-gap crossover takes place and the energy difference of the VBM/CBM at **Γ** [E(**Γ**)] and **K** [E(**K**)] at 0% strain of $MoSe_2$, WSe_2, and BN monolayer. The energies are in eV.

System	Strain percentage	E(**Γ**) − E(**K**)
$MoSe_2$ monolayer	∼3%	0.365 (VBM)
WSe_2 monolayer	∼3%	0.420 (VBM)
BN monolayer	∼2%	−0.094 (CBM)

TABLE IV. Deformation potentials for MoS_2 and ZnO monolayers calculated for the highest occupied band (HOB) and lowest unoccupied band (LUB) at the high-symmetry points indicated. The ionic radii of atoms have been used to calculate the volume of the monolayers.

System	Frac. change in volume	k point	Eigenvalue 0%	Eigenvalue 2%	$dE/(dV/V)$
MoS_2 monolayer	2.005	K-HOB	−2.937	−3.198	−7.685
		K-LUB	−1.179	−1.658	−14.064
		G-HOB	−3.053	−3.055	−0.065
		G-LUB	−0.095	−0.462	−10.805
ZnO monolayer	0.882	K-HOB	−5.605	−5.6413	−0.908
		K-LUB	2.855	2.614	−5.974
		G-HOB	−4.98	−5.188	−5.147
		G-LUB	−2.267	−2.518	−6.216

points, one finds that while the value is small for the highest occupied band (HOB) at the **Γ** point, it is large for that at the **K** point. Hence the crossover in MoS_2 is brought about by a faster moving highest occupied band at the **K** point. These ideas are consistent with the tight-binding analysis presented earlier in the text, where we have Mo d–Mo d interactions strongly affected by strain. These interactions comprise the dominant contribution at the K point, and so we see the highest occupied band at K moving faster than the one at the Γ point. Similar differences in deformation potentials could be seen in ZnO also, where the highest occupied band at the **Γ** point moves faster than the corresponding band at the **K** point. However, the change is not enough to bring the crossover. We also give the corresponding values of the deformation potentials for the lowest unoccupied band (LUB) also for the symmetry points Γ and K.

IV. CONCLUSION

We have considered one monolayer of two semiconductors MoS_2 and ZnO both of which exhibit a direct to indirect band-gap transition under biaxial tensile strain. While a small biaxial tensile strain of 0.83% drives the transition in MoS_2, a much larger biaxial tensile strain of 8% is required in the case of ZnO. This is traced to the nature of interactions determining the highest occupied band at the **Γ** and **K** points. While Mo d–S p interactions contribute to the VBM at the **Γ** point, Mo d–Mo d interactions contribute to the VBM at the **K** point. Strain modifies the hopping interaction strengths and therefore brings about the transformation from a direct band-gap material to an indirect band-gap material. A scaling of the hopping interaction strengths according to Harrison's scaling law [20] within a tight-binding model for MoS_2 is able to capture the effect. In ZnO as the VBM at both symmetry points is determined by Zn d–O p interactions, the scaling is not as effective and requires a much larger strain to bring about the transition. Hence a simple design principle emerges in the choice of systems for band-gap engineering by strain.

ACKNOWLEDGMENTS

P.M. and B.R. thank the Nanomission, Department of Science and Technology, India for support as well as the Unit of Nano Science and Nanotechnology, SN Bose National Centre for Basic Sciences. R.D. and S.D. thank the Council of Scientific and Industrial Research, India.

[1] K. S. Novoselov, A. K. Geim, S. V. Morozov, D. Jiang, Y. Zhang, S. V. Dubonos, I. V. Grigorieva, and A. A. Firsov, Science **306**, 666 (2004).
[2] A. H. C. Neto, F. Guinea, N. M. R. Peres, K. S. Novoselov, and A. K. Geim, Rev. Mod. Phys. **81**, 109 (2009).
[3] Y. Wu, Y.-M. Lin, A. A. Bol, K. A. Jenkins, F. Xia, D. B. Farmer, Y. Zhu, and Ph. Avouris, Nature (London) **472**, 74 (2011).
[4] Y.-M. Lin, K. A. Jenkins, A. Valdes-Garcia, J. P. Small, D. B. Farmer, and Ph. Avouris, Nano Lett. **9**, 422 (2009).
[5] Y.-M. Lin, C. Dimitrakopoulos, K. A. Jenkins, D. B. Farmer, H.-Y. Chiu, A. Grill, and Ph. Avouris, Science **327**, 662 (2010).
[6] X. Miao, S. Tongay, M. K. Petterson, K. Berke, A. G. Rinzler, B. R. Appleton, and A. F. Hebard, Nano Lett. **12**, 2745 (2012).
[7] B. Radisavljevic, A. Radenovic, J. Brivio, V. Giacometti, and A. Kis, Nat. Nanotechnol. **6**, 147 (2011).
[8] Y. Zhang, J. Ye, Y. Matsuhashi, and Y. Iwasa, Nano Lett. **12**, 1136 (2012).
[9] Z. Yin, Hai Li, Hong Li, L. Jiang, Y. Shi, Y. Sun, G. Lu, Q. Zhang, X. Chen, and H. Zhang, ACS Nano **6**, 74 (2012).
[10] H. Fang, S. Chuang, T. C. Chang, K. Takei, T. Takahashi, and A. Javey, Nano Lett. **12**, 3788 (2012).
[11] G. L. Frey, S. Elani, M. Homyonfer, Y. Feldman, and R. Tenne, Phys. Rev. B **57**, 6666 (1998).
[12] C. Lee, H. Yan, L. E. Brus, T. F. Heinz, J. Hone, and S. Ryu, ACS Nano **4**, 2695 (2010).
[13] A. Splendiani, L. Sun, Y. Zhang, T. Li, J. Kim, C.-Y. Chim, G. Galli, and F. Wang, Nano Lett. **10**, 1271 (2010).
[14] W. S. Yun, S. W. Han, S. C. Hong, I. G. Kim, and J. D. Lee, Phys. Rev. B **85**, 033305 (2012).
[15] B. Rakshit and P. Mahadevan, Appl. Phys. Lett. **102**, 143116 (2013).
[16] J. Feng, X. Qian, C.-W. Huang, and J. Li, Nat. Photonics **6**, 866 (2012).
[17] H. Shi, H. Pan, Y.-W. Zhang, and B. I. Yakobson, Phys. Rev. B **87**, 155304 (2013).
[18] P. Johari and V. B. Shenoy, ACS Nano **6**, 5449 (2012).
[19] S. Horzum, H. Sahin, S. Cahangirov, P. Cudazzo, A. Rubio, T. Serin, and F. M. Peeters, Phys. Rev. B **87**, 125415 (2013).
[20] W. A. Harrison, *Electronic Structure and the Properties of Solids: The Physics of the Chemical Bond* (Dover, New York, 1967).
[21] G. Kresse and J. Furthmüller, Phys. Rev. B **54**, 11169 (1996).
[22] R. Murray and B. Evans, J. Appl. Crystallogr. **12**, 312 (1979).
[23] G. Kresse and D. Joubert, Phys. Rev. B **59**, 1758 (1999).
[24] P. E. Blöchl, Phys. Rev. B **50**, 17953 (1994).
[25] J. P. Perdew, K. Burke, and M. Ernzerhof, Phys. Rev. Lett. **77**, 3865 (1996).

[26] C. L. Pueyo, S. Siroky, S. Landsmann, M. W. E. van den Berg, M. R. Wagner, J. S. Reparaz, A. Hoffmann, and S. Polarz, Chem. Mater. **22**, 4263 (2010).
[27] S. Zh. Karazhanov, P. Ravindran, A. Kjekshus, H. Fjellvåg, and B. G. Svensson, Phys. Rev. B **75**, 155104 (2007); B. Rakshit and P. Mahadevan, Phys. Rev. Lett. **107**, 085508 (2011).
[28] D. Alfé, Comput. Phys. Commun. **180**, 2622 (2009).
[29] A. A. Mostofi, J. R. Yates, Y.-S. Lee, I. Souza, D. Vanderbilt, and N. Marzari, Comput. Phys. Commun. **178**, 685 (2008).
[30] C. Franchini, R. Kovik, M. Marsman, S. Sathyanarayana Murthy, J. He, C. Ederer, and G. Kresse, J. Phys.: Condens. Matter **24**, 235602 (2012).
[31] G. B. Liu, W. Y. Shan, Y. Yao, W. Yao, and D. Xiao, Phys. Rev. B **88**, 085433 (2013).
[32] M. Topsakal, E. Aktürk, and S. Ciraci, Phys. Rev. B **79**, 115442 (2009).
[33] C. Tusche, H. L. Meyerheim, and J. Kirschner, Phys. Rev. Lett. **99**, 026102 (2007).